

The $s\pm$ pairing symmetry from electron-phonon coupling in $\text{La}_3\text{Ni}_2\text{O}_7$ under pressure

Yucong Yin,¹ Jun Zhan,^{2,3} Boyang Liu,^{1,*} and Xinloong Han^{4,5,†}

¹*Institute of Theoretical Physics, School of Physics and Optoelectronic Engineering, Beijing University of Technology, Beijing, 100124, China*

²*Beijing National Laboratory for Condensed Matter Physics and Institute of Physics, Chinese Academy of Sciences, Beijing 100190, China*

³*School of Physical Sciences, University of Chinese Academy of Sciences, Beijing 100190, China*

⁴*Department of Physics, Capital Normal University, Beijing 100048, China*

⁵*Kavli Institute for Theoretical Sciences, University of Chinese Academy of Sciences, Beijing 100190, China*

(Dated: April 3, 2026)

The recently discovered bilayer Ruddlesden-Popper nickelate $\text{La}_3\text{Ni}_2\text{O}_7$ exhibits superconductivity with a remarkable transition temperature $T_c \approx 80$ K under applied pressures above 14.0 GPa. This discovery of new family of high-temperature superconductors has garnered significant attention in the condensed matter physics community. In this work, we assume the this high-temperature superconductor is mediated by phonons and investigate the pairing symmetry in two distinct models: (i) the full-coupling case, where the $\text{Ni-}d_{x^2-y^2}$ and $\text{Ni-}d_{3z^2-r^2}$ orbitals are treated equally in both interlayer and intralayer coupling interactions, and (ii) the half-coupling case, where the intralayer coupling involves only the $d_{x^2-y^2}$ orbital, while the interlayer coupling is restricted to the $d_{3z^2-r^2}$ orbital. Our calculations reveal that the interlayer coupling favors an $s\pm$ -wave superconducting state, whereas the intralayer coupling promotes an $s++$ -wave symmetry. Additionally, we discuss the implications of pair-hopping interactions on the superconducting properties. These findings provide valuable insights into the pairing mechanisms and symmetry of this newly discovered high-temperature superconductor.

I. INTRODUCTION

The search for a new family of high transition temperature (high- T_c) superconductors remains the central task in the condensed matter community, since the discovery of copper-based high- T_c superconductors[1–4]. Drawing inspiration from the crystal and electronic structures of cuprates, the iron-based superconductors[5–10] and the recent infinite layer nickelate superconductors[11–17] are discovered. Notably, the discovery of superconducting property in bilayer Ruddlesden-Popper nickelate $\text{La}_3\text{Ni}_2\text{O}_7$ (LNO)[18], which exhibits a remarkable transition temperature $T_c \approx 80$ K under high pressure exceeding 14 GPa, has sparked intensive investigation into this novel superconducting material[19–59]. Subsequent studies[19–21] have further confirmed the observation of zero electrical resistance, solidifying LNO as a promising candidate for further exploration in the field of high- T_c superconductivity. Increasing pressure causes the structure to undergo a transition from the orthorhombic structure of the Amam space group to a regular AA-stacking structure of the Fmmm space group. In contrast to the d^9 electronic configuration in cuprates, the normal valence band in LNO manifests the $d^{7.5}$ configuration[18, 20]. The density functional theory (DFT) further reveals that the band structure in the vicinity of the Fermi level under pressure is mainly dominated by the $\text{Ni-}d_{x^2-y^2}$ and $\text{Ni-}d_{3z^2-r^2}$ orbitals[18]. These different features imply the fundamental diverse

pairing symmetry from the cuprates. Interestingly, in addition to superconductivity, the charge/spin density wave, and non-Fermi-liquid behavior are also suggested by transport measurements[18, 20, 30, 53].

A fundamental question in the study of this new family of high- T_c superconductors revolves around elucidating the underlying superconducting mechanism. Current theoretical efforts have predominantly focused on understanding superconductivity in terms of the unique band structure and electronic correlations present in this material. However, recent experimental findings suggest that electron-phonon coupling may play a pivotal role in determining the electronic properties. The ongoing debate among several research groups on the strength of electron-phonon coupling[60–64] (EPC) raises a critical question: What would be the pairing symmetry in pressurized LNO if the superconducting state is indeed mediated by electron-phonon (e -ph) coupling?

To address this question, we present a systematic investigation of the superconducting pairing symmetry within the framework of BCS theory by solving the linearized gap equations in momentum space. Specifically, we introduce and analyze two distinct models: (i) the full-coupling case, where the $\text{Ni-}d_{x^2-y^2}$ and $\text{Ni-}d_{3z^2-r^2}$ orbitals are treated on an equal footing in the interactions, and (ii) the half-coupling case, where the intralayer coupling involves only the $d_{x^2-y^2}$ orbital, while the interlayer coupling is restricted to the $d_{3z^2-r^2}$ orbital. Our calculations reveal that the interlayer coupling favors a spin-singlet $s\pm$ pairing symmetry, whereas the intralayer coupling competes by stabilizing a spin-singlet $s++$ pairing symmetry.

The remainder of this paper is organized as follows. In

* boyangleo@gmail.com

† hanxinloong@gmail.com

the section II, we introduce our two BCS models band model and demonstrate the method to investigate the superconducting pairing symmetry. In the section III and IV, we present the numerical results in the full-coupling case and in the half-coupling case, respectively. In section V, we further discuss the role of pair hopping term in determining the pairing symmetry. Finally, in the section VI we give our further discussions and conclude this paper.

II. MODEL AND METHOD

The low-energy electronic structure of bilayer $\text{La}_3\text{Ni}_2\text{O}_7$, as revealed by DFT calculations and experiments, is predominantly governed by the Ni- $d_{x^2-y^2}$ and $d_{3z^2-r^2}$ orbitals[18, 22–24]. Motivated by this orbital-selective character, we take a minimal bilayer two-orbital model adapted from Ref. [22]. This effective model successfully encapsulates the essential features of the low-energy band structure near the Fermi level, including orbital hybridization effects and interlayer coupling mechanisms. The model reads

$$H_0 = \sum_{\mathbf{k}\sigma} \Psi_{\mathbf{k}\sigma}^\dagger [H_0(\mathbf{k}) - \mu] \Psi_{\mathbf{k}\sigma}, \quad (1)$$

where the basis is defined as $\Psi_\sigma = (c_{tx^2\sigma}, c_{tz^2\sigma}, c_{bx^2\sigma}, c_{bz^2\sigma})^T$ with field operator $c_{\eta\alpha\sigma}$ denotes the annihilation of an electron with spin $\sigma = \uparrow, \downarrow$ in the top ($\eta = t$) or bottom ($\eta = b$) layer. The orbital index x^2 (z^2) labels the Ni- $d_{x^2-y^2}$ ($d_{3z^2-r^2}$) orbital. The chemical potential is denoted by μ . The matrix H_0 is written as

$$H_0(\mathbf{k}) = \begin{pmatrix} T_{\mathbf{k}}^{x^2} & V_{\mathbf{k}} & t_{\perp}^{x^2} & V'_{\mathbf{k}} \\ V_{\mathbf{k}} & T_{\mathbf{k}}^{z^2} & V'_{\mathbf{k}} & t_{\perp}^{z^2} \\ t_{\perp}^{x^2} & V'_{\mathbf{k}} & T_{\mathbf{k}}^{x^2} & V_{\mathbf{k}} \\ V'_{\mathbf{k}} & t_{\perp}^{z^2} & V_{\mathbf{k}} & T_{\mathbf{k}}^{z^2} \end{pmatrix} \quad (2)$$

with

$$T_{\mathbf{k}}^\eta = 2t_1^\eta(\cos k_x + \cos k_y) + 4t_2^\eta \cos k_x \cos k_y + \epsilon^\eta, \quad (3)$$

$$V_{\mathbf{k}} = 2t_3(\cos k_x - \cos k_y), V'_{\mathbf{k}} = 2t_4(\cos k_x - \cos k_y). \quad (4)$$

Here $T^{\eta=x^2, z^2}$ represents the intralayer intraorbital hopping term, while $V_{\mathbf{k}}$ ($V'_{\mathbf{k}}$) demonstrates the interorbital intralayer (interlayer) hopping. $t_{\perp}^{x^2}$ ($t_{\perp}^{z^2}$) denotes the interlayer hopping term in Ni- $d_{x^2-y^2}$ ($d_{3z^2-r^2}$) orbital. The detailed values of hopping parameters t_1^η , t_2^η , t_3 , t_4 can be found in the reference[22]. Fig. 1(a) presents the calculated band structures of the system, while panels (b)-(d) display the corresponding Fermi surfaces at three representative chemical potentials. In addition to the prominent high- T_c superconducting regime near the critical doping level reported in Ref. [18], we systematically investigate two characteristic doping scenarios: (i) a hole-doped regime with $\mu = -0.328\text{eV}$, where the Fermi surface topology exhibits a van Hove singularity, and (ii) an

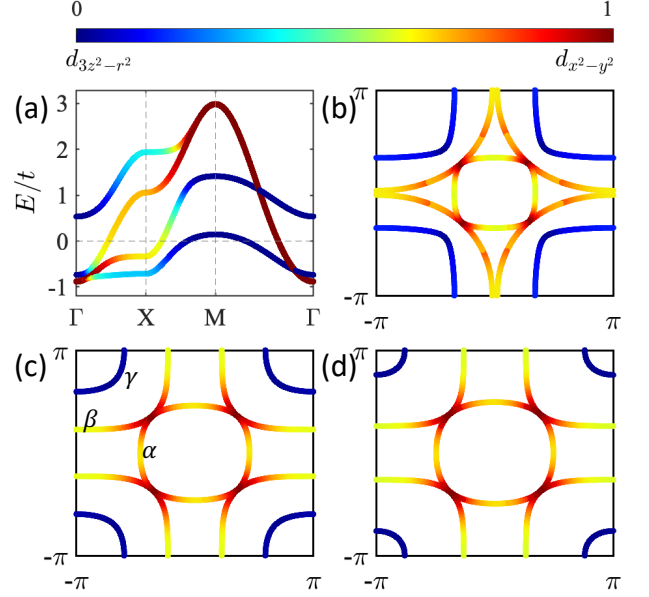


FIG. 1. The orbital-weight band structure[22] (a) and Fermi surfaces (b-d) of the bilayer tight-binding model in the pressured LNO. (b) labels the Fermi surface with $\mu = -0.328\text{eV}$ where it manifest a van Hove singularity. (c) and (d) illustrates the Fermi surface with $\mu = 0\text{eV}$ and 0.1eV , respectively.

electron-doped regime with $\mu = 0.1\text{eV}$. Fig. 1(b-d) reveals that there exist three Fermi surfaces: two hole-like pockets β and γ originating from the interlayer antibonding states of the Ni- $d_{x^2-y^2}$ and bonding state of $d_{3z^2-r^2}$ orbitals; one electron-like pocket formed by the interlayer bonding states of both $d_{x^2-y^2}$ and $d_{3z^2-r^2}$ orbitals. Notably, the orbital-projection analysis demonstrates that the γ pocket predominantly derives its spectral weight from the $d_{3z^2-r^2}$ orbital character.

To elucidate the superconductivity mediated by e -ph coupling in the pressured LNO, we implement two distinct Bardeen-Cooper-Schrieffer (BCS) effective pairing interactions. The first one is the full-coupling case which reads

$$H_I^f = -g_1^f \sum_{\eta\alpha s s'; \mathbf{k}, \mathbf{k}'} \left[c_{\eta\alpha s}^\dagger(\mathbf{k}) c_{\eta\alpha s'}^\dagger(-\mathbf{k}) c_{\eta\alpha s'}(-\mathbf{k}') c_{\eta\alpha s}(\mathbf{k}') \right] - g_2^f \sum_{\alpha s s'; \mathbf{k}, \mathbf{k}'} \left[c_{t\alpha s}^\dagger(\mathbf{k}) c_{b\alpha s'}^\dagger(-\mathbf{k}) c_{b\alpha s'}(-\mathbf{k}') c_{t\alpha s}(\mathbf{k}') \right], \quad (5)$$

in which we take two orbital on equal footing when considering the intralayer or interlayer interactions. The parameters g_1^f and g_2^f represents the intralayer and interlayer pairing strength within the same orbital, respectively, for the full-coupling case. The second type of in-

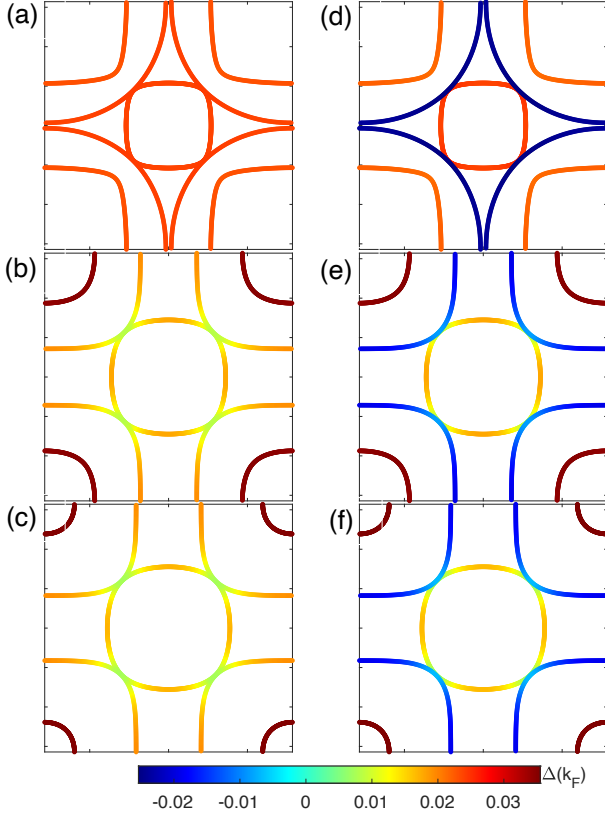


FIG. 2. The pairing gap in the full-coupling case with different parameters. (a), (b) and (c) illustrates the numerical result with only intralayer coupling $g_2^f = 0.12$ for $\mu = -0.328eV$, $0eV$ and $0.1eV$ respectively. (d), (e) and (f) illustrates the numerical result with only interlayer coupling $g_1^f = 0.12$ for $\mu = -0.328eV$, $0eV$ and $0.1eV$ respectively.

interacting Hamiltonian is written as

$$H_I^h = -g_1^h \sum_{\eta s s'; \mathbf{k}, \mathbf{k}'} \left[c_{\eta x^2 s}^\dagger(\mathbf{k}) c_{\eta x^2 s'}^\dagger(-\mathbf{k}) c_{\eta x^2 s'}(-\mathbf{k}') c_{\eta x^2 s}(\mathbf{k}') \right] - g_2^h \sum_{s s'; \mathbf{k}, \mathbf{k}'} \left[c_{t z^2 s}^\dagger(\mathbf{k}) c_{b z^2 s'}^\dagger(-\mathbf{k}) c_{b z^2 s'}(-\mathbf{k}') c_{t z^2 s}(\mathbf{k}') \right], \quad (6)$$

which is referred to as the half-coupling case, where we only consider the intralayer BCS pairing interaction occurring in the $d_{x^2-y^2}$ orbital, while the interlayer BCS pairing interaction occurs in the $d_{3z^2-r^2}$ orbital. The parameter g_1^h (g_2^h) is the intralayer (interlayer) interaction strength. The intralayer interaction in this model is attributed to the coupling of the B_{1g} phonon mode, which involves the in-plane motion of oxygen atoms, to the $d_{x^2-y^2}$ orbital. In contrast, the interlayer interaction is associated with two A_{1g} phonon modes, which are strongly coupled to the $d_{3z^2-r^2}$ orbital. The the low-energy Hamiltonian H is $H = H_0 + H_I^{f,h}$. The orbital and layer basis $c_{\eta\alpha s}(\mathbf{k})$ can be mapped to the band basis

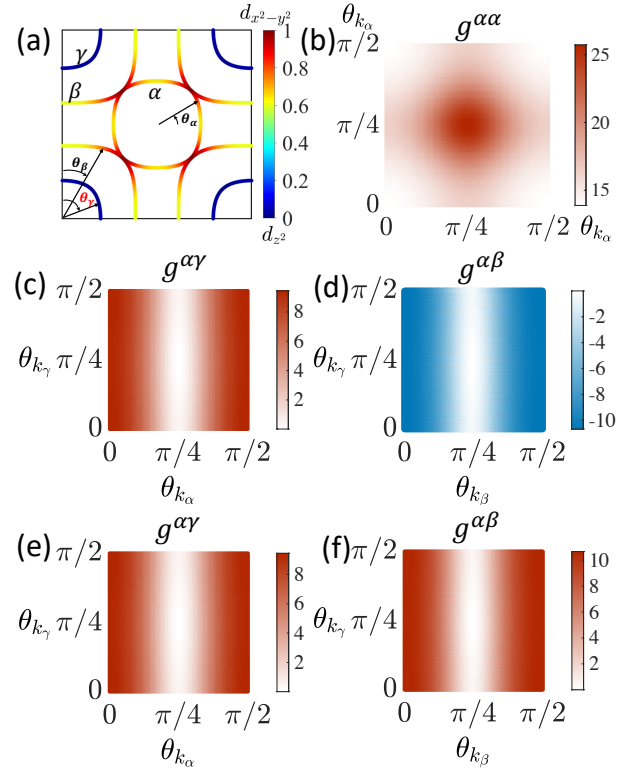


FIG. 3. (a) The momentum distribution at Fermi surfaces when calculating effective interacting strength with fixed $\mu = 0eV$. Effective interacting strength $g^{\alpha\alpha}$ (b), $g^{\alpha\gamma}$ (c) and $g^{\alpha\beta}$ (d) obtained in the full-coupling case with the pure interlayer coupling $g_2^f = 0.12$. Effective interacting strength $g^{\alpha\gamma}$ (e) and $g^{\alpha\beta}$ (f) obtained in the full-coupling case with the pure intralayer coupling $g_1^f = 0.06$.

$c_{bs}(\mathbf{k})$ by introducing a unitary matrix as

$$c_{\eta\alpha s}(\mathbf{k}) = \sum_{\beta} U_{\eta\alpha\beta}(\mathbf{k}) c_{\beta s}(\mathbf{k}) \quad (7)$$

where β is the band index. Here we only consider the intraband pairing, thus the projected interacting Hamiltonian is

$$H_{BCS} = - \sum_{\mathbf{k}, \mathbf{k}'} \sum_{bb'; ss'} g^{\beta, \beta'}(\mathbf{k}, \mathbf{k}') c_{\beta s}^\dagger(\mathbf{k}) c_{\beta s'}^\dagger(-\mathbf{k}) \times c_{\beta' s'}(-\mathbf{k}') c_{\beta' s}(\mathbf{k}') \quad (8)$$

and we define $g^{\beta, \beta'}(\mathbf{k}, \mathbf{k}') = g_1^{\beta, \beta'}(\mathbf{k}, \mathbf{k}') + g_2^{\beta, \beta'}(\mathbf{k}, \mathbf{k}')$ where $g_1^{\beta, \beta'}$ and $g_2^{\beta, \beta'}$ comes from the contribution of the intralayer and interlayer, respectively. Within the mean-field approximation, we introduce the order parameters $\Delta_{ss'}^\beta(\mathbf{k})$ by the following

$$\Delta_{ss'}^{(\beta)}(\mathbf{k}) \equiv \sum_{\beta'} \sum_{\mathbf{k}'} g^{\beta, \beta'}(\mathbf{k}, \mathbf{k}') \langle c_{\beta' s'}(-\mathbf{k}') c_{\beta' s}(\mathbf{k}') \rangle. \quad (9)$$

To get the gap equation, we introduce the Bogoliubov

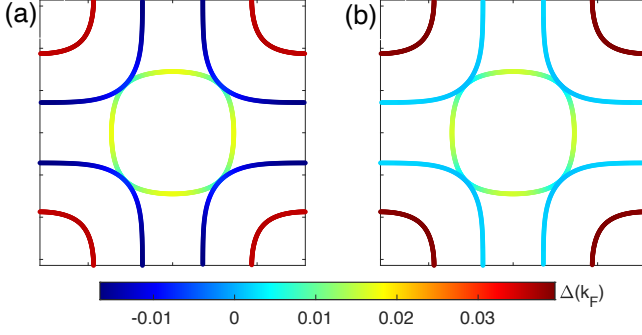


FIG. 4. The pairing gap with fixed interlayer coupling $g_2^f = 0.12$ while varying intralayer coupling $g_1^f = 0.006$ (a) and 0.072 (b) in the full-coupling case with chemical potential $\mu = 0$.

quasiparticles $a_\beta(\mathbf{k})$ and $a_\beta^\dagger(-\mathbf{k})$ and they can be connected to original creation and annihilation operators $c_\beta(\mathbf{k})$ by the following Bogoliubov transformation

$$c_{\beta\uparrow}(\mathbf{k}) = u_{\beta\mathbf{k}}a_{\beta}(\mathbf{k}) + v_{\beta\mathbf{k}}a_{\beta}^\dagger(-\mathbf{k}), \quad (10)$$

$$c_{\beta\downarrow}^\dagger(-\mathbf{k}) = -v_{\beta\mathbf{k}}a_{\beta}(-\mathbf{k}) + u_{\beta\mathbf{k}}a_{\beta}^\dagger(\mathbf{k}), \quad (11)$$

with parameters

$$u_{\beta\mathbf{k}}^2 = \frac{1}{2} \left(1 + \frac{\varepsilon_\beta(\mathbf{k})}{E_\beta(\mathbf{k})} \right), v_{\beta\mathbf{k}}^2 = \frac{1}{2} \left(1 - \frac{\varepsilon_\beta(\mathbf{k})}{E_\beta(\mathbf{k})} \right), \quad (12)$$

where $\varepsilon_\beta(\mathbf{k})$ denotes β -band's energy and $E_\beta(\mathbf{k}) = \sqrt{\varepsilon_\beta^2(\mathbf{k}) + |\Delta_{ss'}^{(\beta)}(\mathbf{k})|^2}$ is the energy of Bogoliubov quasiparticle. Putting Eq. (10-12) into Eq. 9, one can derive the linear gap equations which read

$$\Delta^\beta(\mathbf{k}) = \frac{1}{A} \sum_{\beta', \mathbf{k}'} \chi^{\beta, \beta'}(\mathbf{k}, \mathbf{k}') \Delta^{\beta'}(\mathbf{k}'), \quad (13)$$

with

$$\chi_{\mathbf{k}, \mathbf{k}'}^{(\beta, \beta')} = g^{\beta, \beta'}(\mathbf{k}, \mathbf{k}') \frac{\tanh \left[\frac{\varepsilon_{\beta'}(\mathbf{k}')}{2k_B T} \right]}{2\varepsilon_{\beta'}(\mathbf{k}')}, \quad (14)$$

near the superconducting transition temperature T_c . The superconducting transition temperature T_c is the highest temperature such that the matrix $\chi_{\mathbf{k}, \mathbf{k}'}^{(\beta, \beta')}$ yields eigenvalue 1 in the discrete momentum and band spanned space[65].

III. SUPERCONDUCTING STATE FOR THE FULL-COUPLING CASE

We begin by systematically analyzing the full-coupling case defined in Eq. 5. In the band space, the interacting strength $g_1^{\beta, \beta'}(\mathbf{k}, \mathbf{k}')$ from the contribution of intralayer

coupling is

$$g_1^{\beta, \beta'}(\mathbf{k}, \mathbf{k}') = g_1^f \sum_{\eta\alpha} U_{\eta\alpha}^*(\mathbf{k}) U_{\eta\alpha}^*(-\mathbf{k}) U_{\eta\alpha\beta'}(-\mathbf{k}') \times U_{\eta\alpha\beta'}(\mathbf{k}'), \quad (15)$$

and $g_2^{\beta, \beta'}(\mathbf{k}, \mathbf{k}')$ contributed by the interlayer coupling is

$$g_2^{\beta, \beta'}(\mathbf{k}, \mathbf{k}') = g_2^f \sum_{\alpha} U_{t\alpha\beta}^*(\mathbf{k}) U_{b\alpha\beta}^*(-\mathbf{k}) U_{b\alpha\beta'}(-\mathbf{k}') \times U_{t\alpha\beta'}(\mathbf{k}'). \quad (16)$$

After putting $g^{\beta, \beta'}(\mathbf{k}, \mathbf{k}') = g_1^{\beta, \beta'}(\mathbf{k}, \mathbf{k}') + g_2^{\beta, \beta'}(\mathbf{k}, \mathbf{k}')$ into Eq. (14), we can numerically obtain the pairing gap by solving Eq. (9) and (14).

To clearly understand the role of intralayer and interlayer coupling in the pairing symmetry, we separately examine the intralayer and interlayer couplings and plot the resulting pairing symmetries for various doping levels in Fig. 2. Fig. 2(d-f) show that the pairing symmetry induced by the interlayer BCS coupling in the full-coupling case results in pairing gaps with the same sign in the α and γ pockets, while the gap between the α and β pockets has the opposite sign, for fixed parameters $g_1^f = 0$ and $g_2^f = 0.12$ under various doping conditions. Thus, our numerical calculations for the full-coupling case with only the interlayer coupling indicate that the superconducting state hosts an $s\pm$ -wave pairing symmetry. Furthermore, to address the origin of the $s\pm$ pairing symmetry induced by interlayer coupling, we plot the pairing interactions in the band space in Fig. 3(a-c). As illustrate in Fig. 3(a,b), the pairing interaction $g^{\alpha, \alpha}$ and $g^{\alpha, \gamma}$ indicate negative Josephson coupling both within α intra-Fermi pocket and between α and γ Fermi pockets, intriguing to pairing gaps with the same sign within the same Fermi pockets and between α and γ Fermi pockets. Meanwhile, the negative $g^{\alpha, \beta}$ will favor the opposite sign pairing gap between α and γ Fermi pockets. Conversely, the pure intralayer coupling scenario will sustains the conventional $s++$ -wave superconducting state with uniform pairing gap across all pockets as shown in Fig. 2(a-c) with fixed parameter $g_1^f = 0.12$ and $g_2^f = 0$.

The competition between these two pairing channels manifests a superconducting phase transition in the (g_1^f, g_2^f) parameter space. Fig. 4 explicitly demonstrates that increasing the intralayer coupling strength g_1^f drives a phase transition from the $s\pm$ -wave to $s++$ -wave superconducting ground state, marked by the suppression of inter-pocket gap sign reversal.

IV. PAIRING SYMMETRY IN HALF-COUPLING CASE

In this section, we further investigate the superconducting pairing symmetry in half-coupling case which is demonstrated in Eq. 6. In this case the interaction strength $g^{\beta, \beta'}$ is followed by

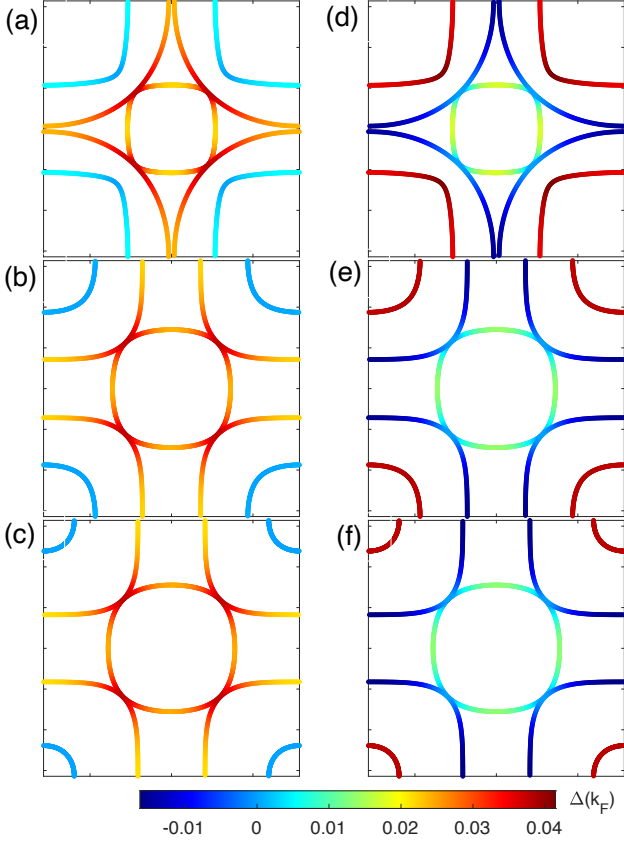


FIG. 5. The pairing gap in the half-coupling case with different parameters. (a), (b) and (c) illustrates the numerical result with only intralayer coupling $g_1^f = 0.18$ for $\mu = -0.328eV, 0eV$ and $0.1eV$ respectively. (d), (e) and (f) illustrates the numerical result with only interlayer coupling $g_2^f = 0.18$ for $\mu = -0.328eV, 0eV$ and $0.1eV$ respectively.

$$g_1^{\beta,\beta'}(\mathbf{k}, \mathbf{k}') = g_1^h \sum_{\eta} U_{\eta x^2\beta}^*(\mathbf{k}) U_{\eta x^2\beta}^*(-\mathbf{k}) U_{\eta x^2\beta'}(-\mathbf{k}') \\ \times U_{\eta x^2\beta'}(\mathbf{k}'), \quad (17)$$

and $g_2^{\beta,\beta'}(\mathbf{k}, \mathbf{k}')$ contributed by the interlayer coupling is

$$g_2^{\beta,\beta'}(\mathbf{k}, \mathbf{k}') = g_2^h U_{tz^2\beta}^*(\mathbf{k}) U_{bz^2\beta}^*(-\mathbf{k}) U_{bz^2\beta'}(-\mathbf{k}') U_{t\alpha\beta'}(\mathbf{k}'). \quad (18)$$

where $g_{1,2}^h$ is the intralayer or interlayer pairing strength in the half coupling case as mentioned before.

Following the methodology employed in the full-coupling scenario, we systematically investigate the individual effects of intralayer and interlayer couplings. By numerically solving the self-consistent equations Eq. (9) and (14) with the interaction $g^{\beta,\beta'}$, we plot the pairing gaps in Fig. 5. As shown in Fig. 5(d-f) with fixed parameters $g_1^h = 0$ and $g_2^h = 0.18$ with several doping conditions, the interlayer coupling also favors the $s\pm$ -wave

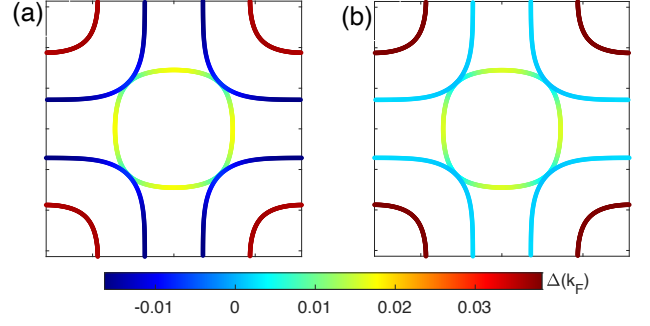


FIG. 6. The pairing gap in the half-coupling case with fixed interlayer coupling $g_2^h = 0.18$ while varying intralayer coupling $g_1^h = 0.016$ (a) and 0.05 (b) with chemical potential $\mu = 0$

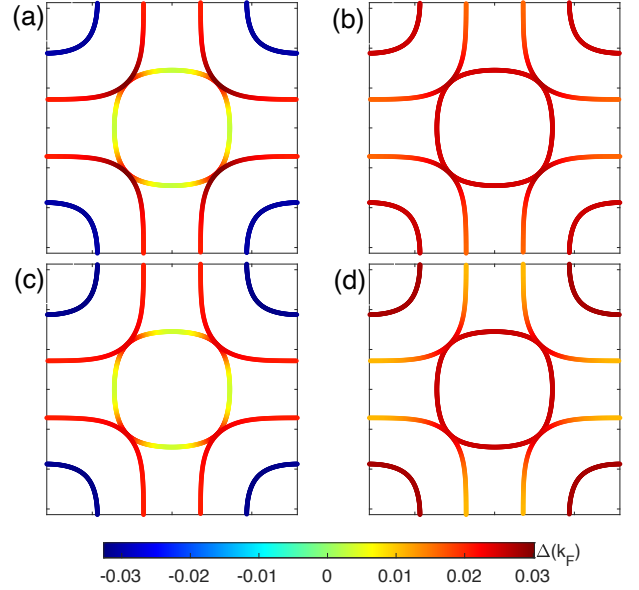


FIG. 7. The pairing gaps with fixed $\mu = 0eV$. (a) and (b) marks the pairing gap in the full-coupling case with fixed parameters $g_1^f = 0.006$ and $g_2^f = 0.12$ while varying pair hopping $g_P = -0.1$ and 0.1 , respectively. (c) and (d) illustrates the pairing gap in the half-coupling case with fixed parameters $g_1^h = 0.016$ and $g_2^h = 0.18$ while varying pair hopping $g_P = -0.1$ and 0.1 , respectively.

pairing symmetry as the same as in the full-coupling case. In Fig. 5(a-c), we use the different intralayer coupling strengths g_2^h to drive the superconducting state and obtain the pairing gap under different doping conditions. Then we reach the same conclusion in the half-coupling case as in the full-coupling scenario, the intralayer coupling g_2^h also tends to induce the conventional $s++$ -wave pairing symmetry, due to the same reasons as discussed in the full-coupling case.

V. THE ROLE OF PAIR HOPPING INTERACTION

In multiband superconductivity, a pertinent question arises regarding the role of the pair-hopping term. To address this, we investigate the pairing symmetry by incorporating the pair-hopping term in both full and half-coupling scenarios. The pair hopping term reads

$$H_P = -g_P \sum_{\eta; \mathbf{k}, \mathbf{k}'; s, s'} c_{\eta x^2 s}^\dagger(-\mathbf{k}) c_{\eta x^2 s'}^\dagger(\mathbf{k}) c_{\eta z^2 s'}(\mathbf{k}') \times c_{\eta z^2 s}(-\mathbf{k}') \quad (19)$$

where g_P is the pair hopping strength. In the band space, it can be rewritten as

$$H_P = - \sum_{\mathbf{k}, \mathbf{k}'} \sum_{\beta \beta'; s s'} g_P^{\beta, \beta'}(\mathbf{k}, \mathbf{k}') c_{\beta s}^\dagger(\mathbf{k}) c_{\beta s'}^\dagger(-\mathbf{k}) \times c_{\beta' s'}(-\mathbf{k}') c_{\beta' s}(\mathbf{k}') \quad (20)$$

with

$$g_P^{\beta, \beta'}(\mathbf{k}, \mathbf{k}') = g_P \sum_{\eta} U_{\eta x^2 \beta}^*(\mathbf{k}) U_{\eta z^2 \beta}^*(-\mathbf{k}) U_{\eta x^2 \beta'}(-\mathbf{k}') \times U_{\eta z^2 \beta'}(\mathbf{k}') \quad (21)$$

Then we can obtain

$$g^{\beta, \beta'} = g_1^{\beta, \beta'}(\mathbf{k}, \mathbf{k}') + g_2^{\beta, \beta'}(\mathbf{k}, \mathbf{k}') + g_P^{\beta, \beta'}(\mathbf{k}, \mathbf{k}') \quad (22)$$

Compared to Fig.4(a), the numerical results presented in Fig.7(a) in the full-coupling model indicate that a negative pair-hopping interaction g_P tends to drive the superconducting state toward an alternative $s\pm$ -wave state. In this state, the pairing gap on the α Fermi surface shares the same sign as the gap on the β Fermi surface but has the opposite sign compared to the gap on the γ Fermi surface. In contrast, a positive g_P in the full-coupling case favors the conventional $s++$ -wave pairing symmetry. The preference for $s\pm$ -wave symmetry by negative and $s++$ -wave symmetry by positive g_P can be attributed to the fact that the Fermi surface is primarily composed of $d_{3z^2-r^2}$ orbital weight, while both the α and β Fermi surfaces have significant contributions from the $d_{x^2-y^2}$ orbital. Fig. 7 (c) and (d) lead to the conclusion that in the half-coupling case the pair-hopping strength g_P plays a similar role as in the full-coupling case.

VI. DISCUSSIONS AND CONCLUSIONS

Our numerical results demonstrate that two coupling constant both need to exceed a finite critical value to get superconducting state (see Appendix B). To our best knowledge, the largest value of EPC constant λ in LNO is estimated to be 1.75 under a pressure of 22.4 GPa[60]. The EPC constant, in combination with a typical Coulomb pseudopotential of $\mu^* \simeq 0.1$, is

sufficient to generate a superconducting state within the McMillan framework. Furthermore, according to DFT calculations[64], the dominant contributions to the phonon spectrum arise from two out-of-plane A_{1g} modes, which are associated with interlayer electron-phonon coupling. Assuming, for simplicity, that these two modes contribute equally to the λ , the interlayer coupling g_2 can be estimated as $g_2/A \sim \lambda/\rho(0)/A \simeq 0.6eV$ where $\rho(0) \simeq 10eV^{-1}nm^{-2}$ is the density of state at $\mu = 0$. This estimated g_2/A exceeds the typical interlayer antiferromagnetic exchange interaction $J_\perp \sim 0.32eV$ [51], and can be comparable to or even surpass the effective suppression from the onsite Hubbard U when projected onto the interlayer pairing channel. Therefore, an interlayer phonon-mediated attraction strong enough to dominate over the residual repulsion is physically plausible.

In summary, we have systematically investigated the superconducting pairing symmetry mediated by effective attractive interactions in the celebrated high-temperature superconductor material $La_3Ni_2O_7$ under pressure. We considered two models, namely the full-coupling case in which the $Ni-d_{x^2-y^2}$ orbital and $d_{3z^2-r^2}$ orbital are treated equally in the interlayer and intralayer interactions, and the half-coupling case where the interlayer and intralayer coupling only includes $d_{3z^2-r^2}$ and $d_{x^2-y^2}$ orbital, respectively. By solving the linear gap equation numerically, we have found that in the both cases the interlayer coupling tends to trigger the $s\pm$ superconducting state with a sign change between β and α (γ) Fermi surfaces, while the intralayer coupling leads to a pure $s++$ -wave without sign change between Fermi surfaces. Hence our calculations have revealed the competitive effect between interlayer and intralayer coupling, and also uncover that the final pairing symmetry arise from the nature of electronic wave-functions near Fermi level of the material under pressure. In addition, we also have considered the pair hopping interaction between $d_{3z^2-r^2}$ and $d_{x^2-y^2}$ orbitals, and have demonstrated that the repulsive pair hopping favors the $s\pm$ pairing symmetry as expected due to the fact γ and α Fermi surface mainly is mainly contributed from the $d_{3z^2-r^2}$ and $d_{x^2-y^2}$, respectively.

VII. ACKNOWLEDGE

We thank Xianxin Wu for very helpful discussions. Xinloong Han is supported by National Natural Science Foundation of China (Grant No. 12404162). Yucong Yin and Boyang Liu are supported by the National Science Foundation of China (Grant No. NSFC-11874002).

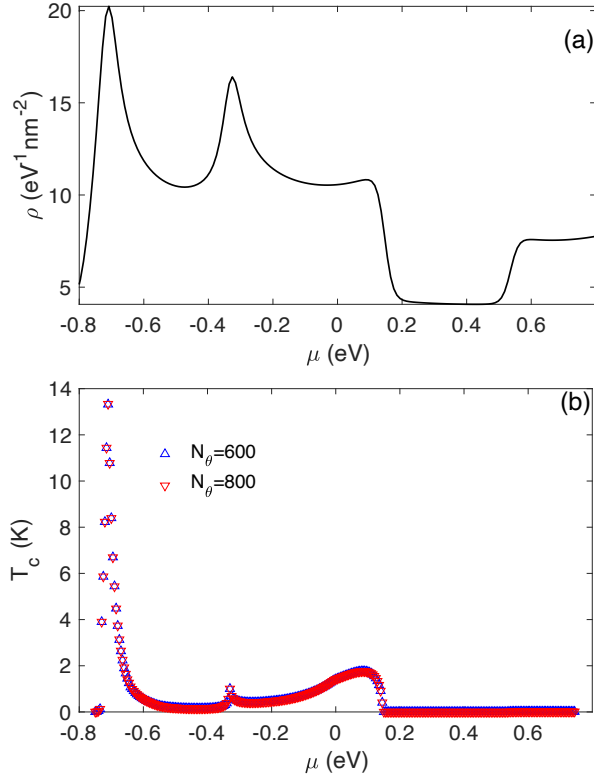


FIG. 8. The density of state ρ (a) and the transition temperature T_c (b) as a function of chemical potential μ . In (b), the blue upward triangles and red downward triangles correspond to calculations using $N_\theta = 600$ and $N_\theta = 800$ in the half-coupling case, respectively. (b) is calculated with parameters $g_1^h = 0$, $g_2^h = 0.18$ and $g_P = 0$.

VIII. APPENDIX

A. Numerical details

To numerically solve the gap equations Eq. (13) in the main text, we firstly rewrite it in the polar coordination and only consider momentum near the Fermi surfaces,

$$\Delta^\beta(\theta) = \sum_{\beta'} \int_0^{2\pi} \frac{d\theta'}{(2\pi)^2} \chi_{\theta, \theta'}^{\beta, \beta'} \Delta^{\beta'}(\theta'), \quad (23)$$

with

$$\chi_{\theta, \theta'}^{\beta, \beta'} = g^{\beta, \beta'}(\theta, \theta') \int_{|\varepsilon_{\beta'}(k_{\theta'})| < \Lambda} k_{\theta'} dk_{\theta'} \frac{\tanh \left[\frac{\varepsilon_{\beta'}(\mathbf{k}')}{2k_B T} \right]}{2\varepsilon_{\beta'}(\mathbf{k}')} \quad (24)$$

where Λ is the energy cutoff. In this paper, we set $\Lambda = 0.15eV$. We also take the equiangular division with N_θ pieces. In Fig. 8(b), In Fig. 8(b), the numerical results obtained with $N_\theta = 600$ and $N_\theta = 800$ are nearly identical, indicating convergence. Therefore, we choose $N_\theta = 600$, unless otherwise specified in this paper.

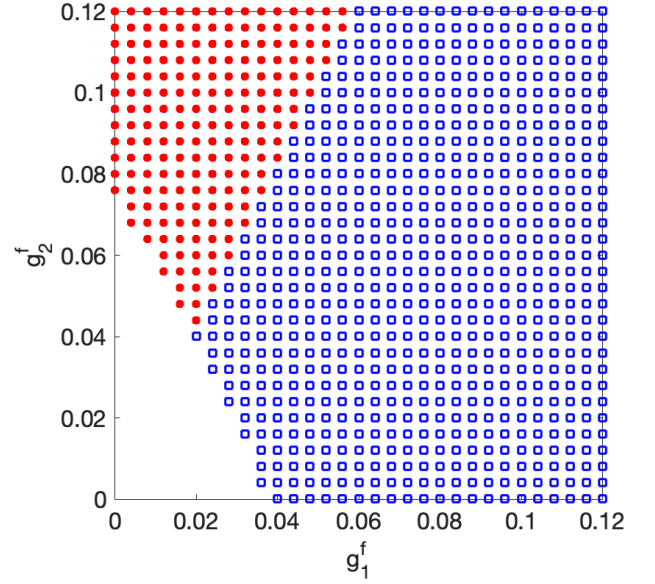


FIG. 9. The phase diagram for the full-coupling case with $g_P = 0$. The blue square denote the conventional s -wave pairing symmetry while the red dot represents the $s\pm$ -wave pairing symmetry. The blank (or white) region indicates that no superconductivity emerges within our lowest accessible temperature range.

B. Phase diagrams

To get a better understanding how intralayer and interlayer coupling compete in both cases, in this section we calculate the phase diagrams for the full-coupling and half-coupling cases. As illustrated in Fig. (9), The phase diagram reveals that s -wave superconductivity dominates a wide region of parameter space, while the $s\pm$ -wave superconductivity phase only appears in a relatively narrow region where the interlayer interaction is significantly weaker than the intralayer interaction. Conversely, $s\pm$ -wave superconductivity in the phase diagram shown in Fig. 10 for the half-coupling case, occupies the vast majority of the parameter space, demonstrating its robust nature. From Fig. (9) and (10), we also notice that the interlayer and intralayer coupling strength in both cases must exceed their critical values to get the superconducting state.

[1] J. G. Bednorz and K. A. Müller, Possible high T_c superconductivity in the Ba-La-Cu-O system, *Z. Phys. B*

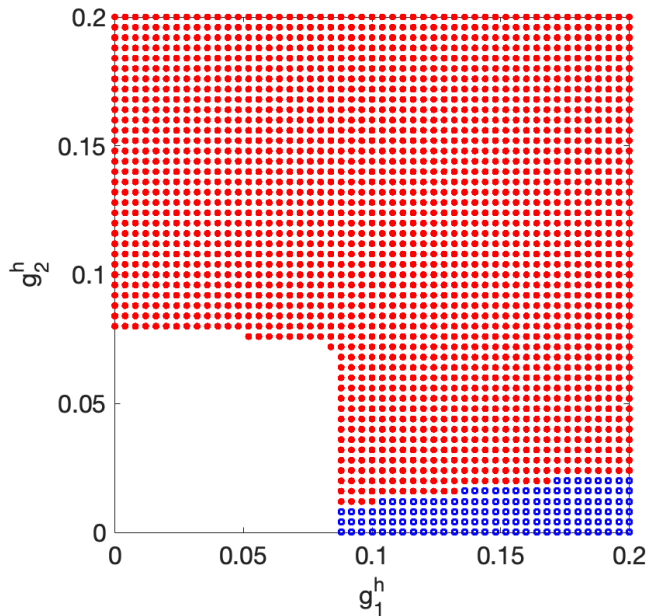


FIG. 10. The phase diagram for the half-coupling case with $g_P = 0$. The blue square denote the conventional s-wave pairing symmetry while the red dot represents the s_{\pm} -wave pairing symmetry.

- [2] P. W. Anderson, The resonating valence bond state in La_2CuO_4 and superconductivity, *Science* **235**, 1196–1198 (1987).
- [3] P. A. Lee, N. Nagaosa, and X.-G. Wen, Doping a Mott insulator: Physics of high-temperature superconductivity, *Rev. Mod. Phys.* **78**, 17–85 (2006).
- [4] B. Keimer, S. A. Kivelson, M. R. Norman, S. Uchida, and J. Zaanen, From quantum matter to high-temperature superconductivity in copper oxides, *Nature* **518**, 179–186 (2015).
- [5] Y. Kamihara, T. Watanabe, M. Hirano, and H. Hosono, Iron-based layered superconductor $\text{La}[\text{O}_{1-x}\text{F}_x]\text{FeAs}$ ($x = 0.05\text{--}0.12$) with $T_c = 26$ K, *J. Am. Chem. Soc.* **130**, 3296–3297 (2008).
- [6] M. Daghofer, A. Moreo, J. A. Riera, E. Arrighoni, D. J. Scalapino, and E. Dagotto, Model for the Magnetic Order and Pairing Channels in Fe Pnictide Superconductors, *Phys. Rev. Lett.* **101**, 237004 (2008).
- [7] S. Raghu, X.-L. Qi, C.-X. Liu, D. J. Scalapino, and S.-C. Zhang, Minimal two-band model of the superconducting iron oxypnictides, *Phys. Rev. B* **77**, 220503 (2008).
- [8] A. V. Chubukov, D. V. Efremov, and I. Eremin, Magnetism, superconductivity, and pairing symmetry in iron-based superconductors, *Phys. Rev. B* **78**, 134512 (2008).
- [9] H. Eschrig and K. Koepernik, Tight-binding models for the iron-based superconductors, *Phys. Rev. B* **80**, 104503 (2009).
- [10] G. R. Stewart, Superconductivity in iron compounds, *Rev. Mod. Phys.* **83**, 1589–1652 (2011).
- [11] D. Li, K. Lee, B. Yang Wang, M. Osada, S. Crossley, H. R. Lee, Y. Cui, Y. Hikita, and H. Y. Hwang, Superconductivity in an infinite-layer nickelate, *Nature* **572**, 624–627 (2019).
- [12] E. Been, W.-S. Lee, H. Y. Hwang, Y. Cui, J. Zaanen, T. Devereaux, B. Moritz, and C. Jia, Electronic Structure Trends Across the Rare-Earth Series in Superconducting Infinite-Layer Nickelates, *Phys. Rev. X* **11**, 011050 (2021).
- [13] K.-W. Lee and W. E. Pickett, Infinite-layer LaNiO_2 : Ni^{1+} is not Cu^{2+} , *Phys. Rev. B* **70**, 165109 (2004).
- [14] M. Hepting, D. Li, C. J. Jia, H. Lu, E. Paris, Y. Tseng, X. Feng, M. Osada, E. Been, Y. Hikita, et al., Electronic structure of the parent compound of superconducting infinite-layer nickelates, *Nat. Mater.* **19**, 381–385 (2020).
- [15] A. S. Botana and M. R. Norman, Similarities and Differences between LaNiO_2 and CaCuO_2 and Implications for Superconductivity, *Phys. Rev. X* **10**, 011024 (2020).
- [16] X. Wu, D. Di Sante, T. Schwemmer, W. Hanke, H. Y. Hwang, S. Raghu, and R. Thomale, Robust $d_{x^2-y^2}$ -wave superconductivity of infinite-layer nickelates, *Phys. Rev. B* **101**, 060504 (2020).
- [17] M. Jiang, M. Berciu, and G. A. Sawatzky, Critical Nature of the Ni Spin State in Doped NdNiO_2 , *Phys. Rev. Lett.* **124**, 207004 (2020).
- [18] H. Sun, M. Huo, X. Hu, J. Li, Z. Liu, Y. Han, L. Tang, Z. Mao, P. Yang, and B. Wang, Signatures of superconductivity near 80 K in a nickelate under high pressure, *Nature* **621**, 493–498 (2023).
- [19] J. Hou, P. T. Yang, Z. Y. Liu, J. Y. Li, P. F. Shan, L. Ma, G. Wang, N. N. Wang, H. Z. Guo, J. P. Sun, et al., Emergence of high-temperature superconducting phase in the pressurized $\text{La}_3\text{Ni}_2\text{O}_7$ crystals (2023), *Chin. Phys. Lett.* **40**, 117302 (2023).
- [20] Y. Zhang, D. Su, Y. Huang, Z. Shan, H. Sun, M. Huo, K. Ye, J. Zhang, Z. Yang, Y. Xu, et al., High-temperature superconductivity with zero resistance and strange-metal behaviour in $\text{La}_3\text{Ni}_2\text{O}_{7-\delta}$, *Nat. Phys.* **2024**, 1–5 (2024).
- [21] G. Wang, N. N. Wang, X. L. Shen, J. Hou, L. Ma, L. F. Shi, Z. A. Ren, Y. D. Gu, H. M. Ma, P. T. Yang, et al., Pressure-Induced Superconductivity In Polycrystalline $\text{La}_3\text{Ni}_2\text{O}_{7-\delta}$, *Phys. Rev. X* **14**, 011040 (2024).
- [22] Z. Luo, X. Hu, M. Wang, W. Wu, and D.-X. Yao, Bilayer two-orbital model of $\text{La}_3\text{Ni}_2\text{O}_7$ under pressure, *Phys. Rev. Lett.* **131**, 126001 (2023).
- [23] F. Lechermann, J. Gondolf, S. Bötzel, and I. M. Eremin, Electronic correlations and superconducting instability in $\text{La}_3\text{Ni}_2\text{O}_7$ under high pressure, *Phys. Rev. B* **108**, L201121 (2023).
- [24] Y. Gu, C. Le, Z. Yang, X. Wu, and J. Hu, Effective model and pairing tendency in bilayer Ni-based superconductor $\text{La}_3\text{Ni}_2\text{O}_7$, *arXiv:2306.07275* (2023).
- [25] Q.-G. Yang, D. Wang, and Q.-H. Wang, Possible s_{\pm} -wave superconductivity in $\text{La}_3\text{Ni}_2\text{O}_7$, *Phys. Rev. B* **108**, L140505 (2023).
- [26] V. Christiansson, F. Petocchi, and P. Werner, Correlated electronic structure of $\text{La}_3\text{Ni}_2\text{O}_7$ under pressure, *Phys. Rev. Lett.* **131**, 206501 (2023).
- [27] H. Sakakibara, N. Kitamine, M. Ochi, and K. Kuroki, Possible high T_c superconductivity in $\text{La}_3\text{Ni}_2\text{O}_7$ under high pressure through manifestation of a nearly half-filled bilayer Hubbard model, *Phys. Rev. Lett.* **132**, 106002 (2024).
- [28] D. A. Shilenko and I. V. Leonov, Correlated electronic structure, orbital-selective behavior, and magnetic correlations in double-layer $\text{La}_3\text{Ni}_2\text{O}_7$ under pressure, *Phys. Rev. B* **108**, 125105 (2023).

- [29] Y. Shen, M. Qin, and G.-M. Zhang, Effective bilayer model Hamiltonian and density-matrix renormalization group study for the high- T_c superconductivity in $\text{La}_3\text{Ni}_2\text{O}_7$ under high pressure, *Chin. Phys. Lett.* **40**, 127401 (2023).
- [30] Z. Liu, M. Huo, J. Li, Q. Li, Y. Liu, Y. Dai, X. Zhou, J. Hao, Y. Lu, M. Wang, et al., Electronic correlations and energy gap in the bilayer nickelate $\text{La}_3\text{Ni}_2\text{O}_7$, *Nat. Commun.* **15**, 7570 (2024).
- [31] W. Wú, Z. Luo, D.-X. Yao, and M. Wang, Superexchange and charge transfer in the nickelate superconductor $\text{La}_3\text{Ni}_2\text{O}_7$ under pressure, *Sci. China Phys. Mech. Astron.* **67**, 117402 (2024).
- [32] X. Chen, P. Jiang, J. Li, Z. Zhong, and Y. Lu, Charge and spin instabilities in superconducting $\text{La}_3\text{Ni}_2\text{O}_7$, *Phys. Rev. B* **111**, 014515 (2025).
- [33] Y. Cao and Y.-F. Yang, Flat bands promoted by Hund's rule coupling in the candidate double-layer high-temperature superconductor $\text{La}_3\text{Ni}_2\text{O}_7$ under high pressure, *Phys. Rev. B* **109**, L081105 (2024).
- [34] Y.-B. Liu, J.-W. Mei, F. Ye, W.-Q. Chen, and F. Yang, $s\pm$ -wave pairing and the destructive role of apical-oxygen deficiencies in $\text{La}_3\text{Ni}_2\text{O}_7$ under pressure, *Phys. Rev. Lett.* **131**, 236002 (2023).
- [35] Y. Zhang, L.-F. Lin, A. Moreo, and E. Dagotto, Electronic structure, dimer physics, orbital-selective behavior, and magnetic tendencies in the bilayer nickelate superconductor $\text{La}_3\text{Ni}_2\text{O}_7$ under pressure, *Phys. Rev. B* **108**, L180510 (2023).
- [36] C. Lu, Z. Pan, F. Yang, and C. Wu, Interlayer-Coupling-Driven High-Temperature Superconductivity in $\text{La}_3\text{Ni}_2\text{O}_7$ under Pressure, *Phys. Rev. Lett.* **132**, 146002 (2024).
- [37] Y. Zhang, L.-F. Lin, A. Moreo, T. A. Maier, and E. Dagotto, Structural phase transition, $s\pm$ -wave pairing, and magnetic stripe order in bilayered superconductor $\text{La}_3\text{Ni}_2\text{O}_7$ under pressure, *Nat. Commun.* **15**, 2470 (2024).
- [38] H. Oh and Y.-H. Zhang, Type-II t - J model and shared superexchange coupling from Hund's rule in superconducting $\text{La}_3\text{Ni}_2\text{O}_7$, *Phys. Rev. B* **108**, 174511 (2023).
- [39] Z. Liao, L. Chen, G. Duan, Y. Wang, C. Liu, R. Yu, and Q. Si, Electron correlations and superconductivity in $\text{La}_3\text{Ni}_2\text{O}_7$ under pressure tuning, *Phys. Rev. B* **108**, 214522 (2023).
- [40] X.-Z. Qu, D.-W. Qu, J. Chen, C. Wu, F. Yang, W. Li, and G. Su, Bilayer t - J - J_\perp Model and Magnetically Mediated Pairing in the Pressurized Nickelate $\text{La}_3\text{Ni}_2\text{O}_7$, *Phys. Rev. Lett.* **132**, 036502 (2024).
- [41] Y.-F. Yang, G.-M. Zhang, and F.-C. Zhang, Interlayer valence bonds and two-component theory for high- T_c superconductivity of $\text{La}_3\text{Ni}_2\text{O}_7$ under pressure, *Phys. Rev. B* **108**, L201108 (2023).
- [42] K. Jiang, Z. Wang, and F.-C. Zhang, High-temperature superconductivity in $\text{La}_3\text{Ni}_2\text{O}_7$, *Chin. Phys. Lett.* **41**, 017402 (2024).
- [43] Y. Zhang, L.-F. Lin, A. Moreo, T. A. Maier, and E. Dagotto, Trends in electronic structures and $s\pm$ -wave pairing for the rare-earth series in bilayer nickelate superconductor $\text{R}_3\text{Ni}_2\text{O}_7$, *Phys. Rev. B* **108**, 165141 (2023).
- [44] J. Huang, Z. D. Wang, and T. Zhou, Impurity and vortex states in the bilayer high-temperature superconductor $\text{La}_3\text{Ni}_2\text{O}_7$, *Phys. Rev. B* **108**, 174501 (2023).
- [45] Y.-H. Tian, Y. Chen, J.-M. Wang, R.-Q. He, and Z.-Y. Lu, Correlation effects and concomitant two-orbital $s\pm$ -wave superconductivity in $\text{La}_3\text{Ni}_2\text{O}_7$ under high pressure, *Phys. Rev. B* **109**, 165154 (2024).
- [46] Q. Qin and Y. Yang, High- T_c superconductivity by mobilizing local spin singlets and possible route to higher T_c in pressurized $\text{La}_3\text{Ni}_2\text{O}_7$, *Phys. Rev. B* **108**, L140504 (2023).
- [47] G. Heier, K. Park, and S. Y. Savrasov, Competing d_{xy} and $s\pm$ pairing symmetries in superconducting $\text{La}_3\text{Ni}_2\text{O}_7$: LDA+FLEX calculations, *Phys. Rev. B* **109**, 104508 (2024).
- [48] R. Khasanov, T. J. Hicken, D. J. Gawryluk, L. P. Sorel, S. Bötzel, F. Lechermann, I. M. Eremin, H. Luetkens, Z. Guguchia, Pressure-Induced Split of the Density Wave Transitions in $\text{La}_3\text{Ni}_2\text{O}_{7-\delta}$, [arXiv:2402.10485](https://arxiv.org/abs/2402.10485) (2024).
- [49] Y. Meng, Y. Yang, H. Sun, S. Zhang, J. Luo, L. Chen, X. Ma, M. Wang, F. Hong, X. Wang, Density-wave-like gap evolution in $\text{La}_3\text{Ni}_2\text{O}_7$ under high pressure revealed by ultrafast optical spectroscopy, *Nat. Commun.* **15**, 10408 (2024).
- [50] J. Yang, H. Sun, X. Hu, Y. Xie, T. Miao, H. Luo, H. Chen, B. Liang, W. Zhu, G. Qu, Orbital-dependent electron correlation in double-layer nickelate $\text{La}_3\text{Ni}_2\text{O}_7$, *Nat. Commun.* **15**, 4373 (2024).
- [51] R. Jiang, J. Hou, Z. Fan, Z.-J. Lang, and W. Ku, Pressure Driven Fractionalization of Ionic Spins Results in Cupratelike High- T_c Superconductivity in $\text{La}_3\text{Ni}_2\text{O}_7$, *Phys. Rev. Lett.* **132**, 126503 (2024).
- [52] X.-W. Yi, Y. Meng, J.-W. Li, Z.-W. Liao, W. Li, J.-Y. You, B. Gu, and G. Su, Nature of charge density waves and metal-insulator transition in pressurized $\text{La}_3\text{Ni}_2\text{O}_7$, *Phys. Rev. B* **110**, L140508 (2024).
- [53] Z. Liu, H. Sun, M. Huo, X. Ma, Y. Ji, E. Yi, L. Li, H. Liu, J. Yu, Z. Zhang, et al., Evidence for charge and spin density waves in single crystals of $\text{La}_3\text{Ni}_2\text{O}_7$ and $\text{La}_3\text{Ni}_2\text{O}_6$, *Science China Phys. Mech. Astron.* **66**, 217411 (2023).
- [54] B. Geisler, J. J. Hamlin, G. R. Stewart, R. G. Hennig, and P. J. Hirschfeld, Structural transitions, octahedral rotations, and electronic properties of $\text{A}_3\text{Ni}_2\text{O}_7$ rare-earth nickelates under high pressure, *npj Quantum Mater.* **9**, 38 (2024).
- [55] C. Xia, H. Liu, S. Zhou, H. Chen, Sensitive dependence of pairing symmetry on Ni- e_g crystal field splitting in the nickelate superconductor $\text{La}_3\text{Ni}_2\text{O}_7$, *Nat. Commun.* **16**, 1054 (2025).
- [56] K.-Y. Jiang, Y.-H. Cao, Q.-G. Yang, H.-Y. Lu, Q.-H. Wang, Theory of Pressure Dependence of Superconductivity in Bilayer Nickelate $\text{La}_3\text{Ni}_2\text{O}_7$, *Phys. Rev. Lett.* **134**, 076001 (2025).
- [57] G. Zhou, W. Lv, H. Wang, Z. Nie, Y. Chen, Y. Li, H. Huang, W. Chen, Y. Sun, Q.-K. Xue, Ambient-pressure superconductivity onset above 40 K in $(\text{La}, \text{Pr})_3\text{Ni}_2\text{O}_7$ films, *Nature* (2025).
- [58] Z. Dong, M. Huo, J. Li, J. Li, P. Li, H. Sun, L. Gu, Y. Lu, M. Wang, Y. Wang, et al., Visualization of oxygen vacancies and self-doped ligand holes in $\text{La}_3\text{Ni}_2\text{O}_{7-\delta}$, *Nature* **630**, 847–852 (2024).
- [59] Z. Dan, Y. Zhou, M. Huo, Y. Wang, L. Nie, M. Wang, T. Wu, X. Chen, Spin-density-wave transition in double-layer nickelate $\text{La}_3\text{Ni}_2\text{O}_7$, *Science Bulletin* **70**(8), 1239-1245(2025).
- [60] E. F. Talantsev and V. V. Chistyakov, Debye temperature, electron-phonon coupling constant, and three-dome

- shape of crystalline strain as a function of pressure in highly compressed $\text{La}_3\text{Ni}_2\text{O}_{7-\delta}$, [Letters on Materials](#) **14**, 262 (2024).
- [61] Y. D. Li, Y. T. Cao, L. Y. Liu, P. Peng, H. Lin, C. Y. Pei, M. X. Zhang, H. Wu, X. Du, W. X. Zhao, Ultrafast Dynamics of Bilayer and Trilayer Nickelate Superconductors, [arXiv:2403.05012](#) (2024).
- [62] J.-Y. You, Z. Zhu, M. Del Ben, W. Chen, Z. Li, Unlikelihood of a phonon mechanism for the high-temperature superconductivity in $\text{La}_3\text{Ni}_2\text{O}_7$, [npj Comput. Mater.](#) **11**, 3 (2025).
- [63] Z. Ouyang, M. Gao, Z.-Y. Lu, Absence of electron-phonon coupling superconductivity in the bilayer phase of $\text{La}_3\text{Ni}_2\text{O}_7$ under pressure, [npj Quantum Mater.](#) **9**, 80 (2024).
- [64] J. Zhan, Y. Gu, X. Wu, J. Hu, Cooperation between Electron-Phonon Coupling and Electronic Interaction in Bilayer Nickelates $\text{La}_3\text{Ni}_2\text{O}_7$, [Phys. Rev. Lett.](#) **134**, 136002 (2025).
- [65] Y.-Z. Chou, F. Wu, J. D. Sau, S. Das Sarma, Acoustic-phonon-mediated superconductivity in rhombohedral trilayer graphene, [Phys. Rev. Lett.](#) **127**, 187001 (2021).